Received: 3 July 2023 | Revised: 19 January 2024 | Accepted: 29 January 2024

DOI: 10.1111/ter.12706

RESEARCH ARTICLE

Terra Nova WILEY

# Coupled U–Pb and $^{40}Ar/^{39}Ar$ chronology of late-stage intrusions at Elba Island (Italy) supports late Miocene long-lived magma reservoirs in the Tyrrhenian upper crust

F. Mazzarini[1] | L. Bracciali[2] | G. Musumeci[1,3] | J. R. Wijbrans[4] | K. Kuiper[4] | M. S. A. Horstwood[2]

[1]Istituto Nazionale di Geofisica e Vulcanologia, Pisa, Italy

[2]British Geological Survey, Nottingham, UK

[3]Dipartimento di Scienze della Terra, University of Pisa, Pisa, Italy

[4]Department of Earth Sciences, Vrije Universiteit Amsterdam, Amsterdam, The Netherlands

**Correspondence**
F. Mazzarini, Istituto Nazionale di Geofisica e Vulcanologia, Pisa, Italy.
Email: francesco.mazzarini@ingv.it

## Abstract

The late Miocene Monte Capanne and Porto Azzurro plutons are investigated by means of coupled U–Pb zircon and $^{40}Ar/^{39}Ar$ white mica dating to test the occurrence of long-lived magmatic systems in the upper crust. Zircon crystallized for >1 Ma in both plutonic systems, with supersolidus conditions overlapping for ~220 ka indicating previously unrecognized co-existence of the two reservoirs. The development of the Porto Azzurro high T-aureole is post-dated by continuous igneous zircon crystallization until ~6.0 Ma. By linking crystallization to post-emplacement cooling of late-stage pulses in both western and eastern Elba we constrain long-lived sizeable reservoirs (possibly the same reservoir) in the Tyrrhenian upper crust between ~8 and 6 Ma.

**KEYWORDS**
$^{40}Ar/^{39}Ar$ white mica dating, Elba Island, long-lived magma reservoirs, U–Pb zircon dating, Miocene Tyrrhenian crust, upper crustal granites

## 1 | INTRODUCTION

A large body of geochronological data has shown that many magmatic systems are long-lived (Annen et al., 2015; Bachmann et al., 2007; Jackson et al., 2018; Kaiser et al., 2017; Miller & Paterson, 2001; Wotzlaw et al., 2013).

Late Miocene–Pliocene granite intrusions occurring in the northern Tyrrhenian Sea-northern Apennines (e.g. Dini et al., 2002) have been interpreted to result from an eastward migration of scattered magmatic activity based on early geochronological constraints (e.g. Serri et al., 1993). More recently, high-precision U–Pb dating of the Monte Capanne (MC) pluton (Barboni & Schoene, 2014; Barboni et al., 2015) and the Plio-Pleistocene granites associated with the Larderello geothermal system in southern Tuscany (Farina et al., 2018) has shown that zircon dates in single samples can range from ~200 up to ~500 ka.

At Elba Island, the late Miocene magmatism comprises two large plutons (Monte Capanne and Porto Azzurro, PA; Barboni & Schoene, 2014; Dini et al., 2002; Rocchi et al., 2010; Text S1). The island therefore represents a natural, accessible laboratory to investigate the thermal evolution and temporal relationships between crustal magmatic systems in the wider context of the Miocene post-collisional crustal evolution of the Tyrrhenian domain. We use new absolute (radiogenic) time constraints from U–Pb zircon and $^{40}Ar/^{39}Ar$ white mica dating of late-stage magmatic dykes of the MC and PA plutons and a compilation of literature data to test the presence of long-lived magmatic system in this portion of the Tyrrhenian crust.

## 2 | SIGNIFICANCE OF COUPLED U–Pb ZIRCON—$^{40}Ar/^{39}Ar$ WHITE MICA DATING

To track the thermal evolution of the igneous system across a wide temperature range at Elba Island, from early crystallization in the middle crust to post-emplacement cooling through ~400°C in the upper crust, we have carried out coupled U–Pb zircon and $^{40}Ar/^{39}Ar$ white mica dating on igneous samples.

  

The two minerals exhibit remarkably different behaviour with regards to retention of stable Pb and Ar radiogenic daughter isotopes. Both experimental and empirical studies suggest a nominal 'closure $T$' ($T_c$) of Pb in zircon of ~900°C (Lee et al., 1997). The notion of bulk $T_c$ (Dodson, 1973) defines the boundary between closed-system (radiogenic daughter retention below $T_c$) and open-system behaviour (radiogenic daughter loss above $T_c$). Primary zircon crystallizes from igneous melts typically between ~600 and 900°C, that is at temperatures where Pb diffusion rates are negligibly slow at geological time scales (e.g. Cherniak & Watson, 2000). Hence, unless compromised by metamictization or low-T dissolution–precipitation causing open-system behaviour, concordant zircon U–Pb dates indicate the crystallization age of the mineral (see review in Bracciali, 2019).

Conversely, in white mica and other K-bearing thermochronometers, thermally-induced Ar volume diffusion (assumed to be the dominant process controlling Ar loss) is high at the temperatures encountered in the lower and middle crust (Schaen et al., 2020 and references therein). Hence in samples that preserve high-T petrologic equilibrium, $^{40}Ar/^{39}Ar$ dates commonly reflect cessation of diffusion as the sample cooled. This requires the assumption that samples have retained radiogenic Ar after the mineral cooled below its nominal $T_c$, which, for white mica, has been estimated as ~390°C (Harrison et al., 2009) or higher (~500°C; Villa, 2010), and no diffusion out of the crystal lattice during cooling or subsequent reheating events occurred.

**Significance Statement**

The significant findings of this study are the coupled chronologic high temperature (U/Pb on Zircons) and low temperature ($^{40}Ar/^{39}Ar$ on white mica) dates on late-stage intrusions at Elba Island. These new data indicate that, different from what is known, the two large Miocene plutons, tens of kilometers apart had an overlapping supersolidus condition suggesting the occurrence of a common, long-lived magma reservoir at depth.

## 3 | GEOLOGICAL SETTING

The northern Apennine Cenozoic belt is the result of the continental collision following Oligocene-Miocene subduction of the Adria microplate beneath the European plate (Alpine orogeny). The E-verging northern Apennine thrust stack includes oceanic and continental units (Boccaletti et al., 1971; Conti et al., 2020). Late Miocene magmatism in the northern Apennines is interpreted to result from the rollback of Adria and asthenosphere upwelling (Rosenbaum & Lister, 2004 and references therein). A well-preserved portion of the Apennine tectonic stack intruded by late Miocene plutons is exposed at Elba Island (Figure 1; Text S1).

## 4 | IGNEOUS SYSTEMS AT ELBA ISLAND

The MC is a monzogranitic, slightly peraluminous intrusion resulting from the under-accretion in the shallow crust of three geochemically and petrographically distinct magma batches (the large K-feldspar phenocrysts-rich to -poor facies Sant'Andrea, San Francesco and San Piero; Farina et al., 2010; estimated total volume of ca. 135 $km^3$). High-precision zircon U–Pb dating (by chemical abrasion isotope dilution thermal ionization mass spectrometry, ID-TIMS) of zircon crystals (following removal of CL-imaged inherited cores) testifies to a 200–400 ka zircon crystallization history in each batch. Large part of the zircon crystallization is inferred to have occurred in deep crustal reservoirs based on maximum thermally-modelled melt residence time (at emplacement level) of ~65 ka for any batch (Barboni et al., 2015, their U–Pb data plotted in our Figure 3). This is consistent with modelled zircon saturation of ~800°C, well above the solidus modelled for these melts (688–666°C; Barboni et al., 2015). Barboni et al. (2015) inferred incremental growth of the MC pluton over ~250 ka with limited super-solidus interaction between multiple magma pulse injections.

In western-central Elba, a Late Miocene laccolith system is also exposed (Barboni & Schoene, 2014; Rocchi et al., 2010).

The PA pluton is a buried intrusion emplaced in the lowermost Apenninic metamorphic unit (Monte Calamita unit). Its ~7 km width is inferred based on the E-W diameter of the contact aureole at the surface (Papeschi et al., 2017). The exposed rocks are limited to a monzogranite outcrop (Maineri et al., 2003) and a swarm of leucogranite sheets (Papeschi et al., 2022). High-T metamorphic conditions are documented in the deepest portions of the PA aureole, with migmatite rocks developed at ~700°C (Papeschi et al., 2019).

## 5 | LATE-STAGE INTRUSIONS

The MC and PA plutons are associated with numerous late-magmatic peraluminous leucogranite and aplite-pegmatite dykes (Text S1) and veins (Dini et al., 2002).

We have dated zircon and white mica crystals from two dykes (~1 m thick) associated with the MC pluton (samples MC1 and MC2, respectively aplite and microgranite, Figure 2a,d) intruding the ophiolite host-rock, and a monzogranite apophysis (~20 m thick) cross-cutting the hornfels of the contact metamorphic aureole of the PA pluton (sample PA1, Figure 2g; Figure S1.1). The mineral assemblages of both MC1 and MC2 consist of quartz, K-feldspar, tourmaline, biotite, albite, white mica and show an igneous foliation defined by K-feldspar, white mica and tourmaline (Figure 2b,e; Figure S1.2). Titanite, apatite and zircon occur as accessory phases. PA1 is characterized by a disequigranular, generally isotropic texture formed by quartz, K-feldspar, albite, biotite, tourmaline, white mica, apatite and titanite with phenocrysts of K-feldspar and tourmaline up to a few centimetre in length (Figure 2h).

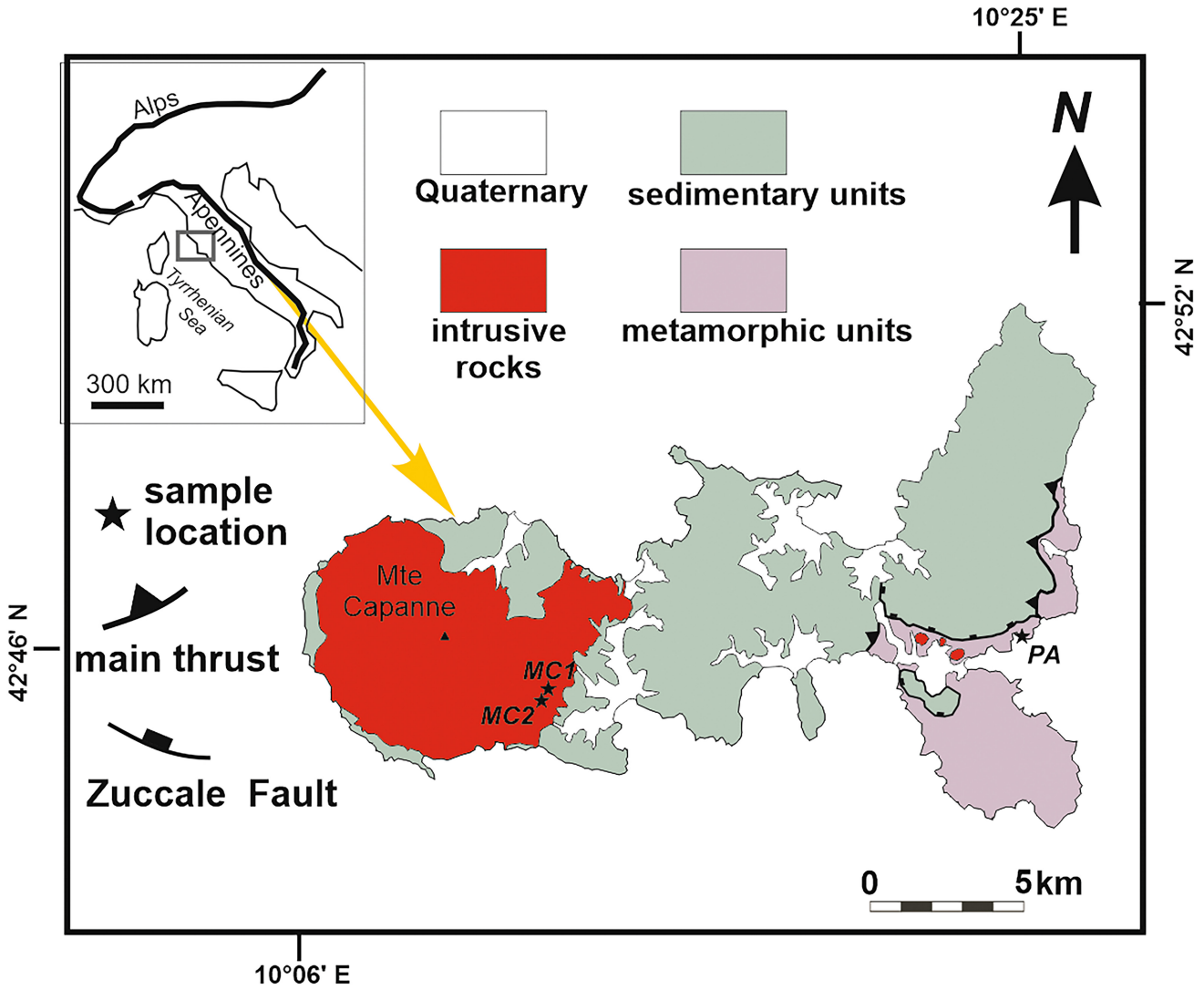


FIGURE 1 Schematic geological map of Elba Island with sample locations. Inset shows: Elba location in the Tyrrhenian Sea west of mainland Italy and a schematic representation of the Eocene Alps-Apennine orogen.

In all samples, magmatic white mica is euhedral to subhedral and ranges from 0.2 to 1 mm. Zircons in all samples exhibit a fine, concentric oscillatory CL-zoning typical of igneous zircons and occasionally present patchy-zoned inherited cores (Figure 2c,f,i; Text S2). Such patchy cores were interpreted by Gagnevin et al. (2011) as a replacement of original U–Th–Y-rich domains by U–Th–Y-poor zircon.

Full details of the mineral separation techniques and the analytical dating methods, LA MC-ICP-MS and noble gas MS, are given in Text S2–S4 and Table S2.

## 6 | RESULTS AND INTERPRETATION

Our U–Pb and $^{40}Ar/^{39}Ar$ results (Tables S3 and S5; Figures S3–S5) are plotted in Figures 3 and 4, along with published data (Table S6). For zircon, only U–Pb data determined on CL-oscillatory zoned domains reflecting igneous crystallization (most commonly 'rims') are plotted and used for the interpretation.

For our <10 Ma U–Pb LA ICP-MS data (indeed remarkably precise thanks to the high U content, estimated in the range of 1000s ppm in all samples, Table S3) the uncertainty on the 6/38 date was <2% (2s). Individual absolute $^{206}Pb/^{238}U$ age uncertainties (2s) were in the range of ±130–140 ka. Similarly, the radiogenic $^{40}Ar$ yields measured in the white mica samples were high (Table S5). Our chronology data are plotted as ranked distributions of individual dates (±2s). High precision (ID-TIMS) U–Pb zircon data from the MC main granite body by Barboni et al. (2015) are plotted as kernel density estimate (KDE) plots. Each of their samples (±8 ka, average uncertainty). The KDE peaks of the MC pluton samples indicate younging of the magma batches, from the top (Sant'Andrea facies) to the bottom (San Piero facies) of the composite MC intrusion. Since previous studies have highlighted the occurrence of zircon age variation (Barboni et al., 2015) and a number of our U–Pb data points repeat well, indicating that potential Pb-loss was limited (which at this age range of interest would be unresolvable, causing data to plot in a line along concordia), we interpret

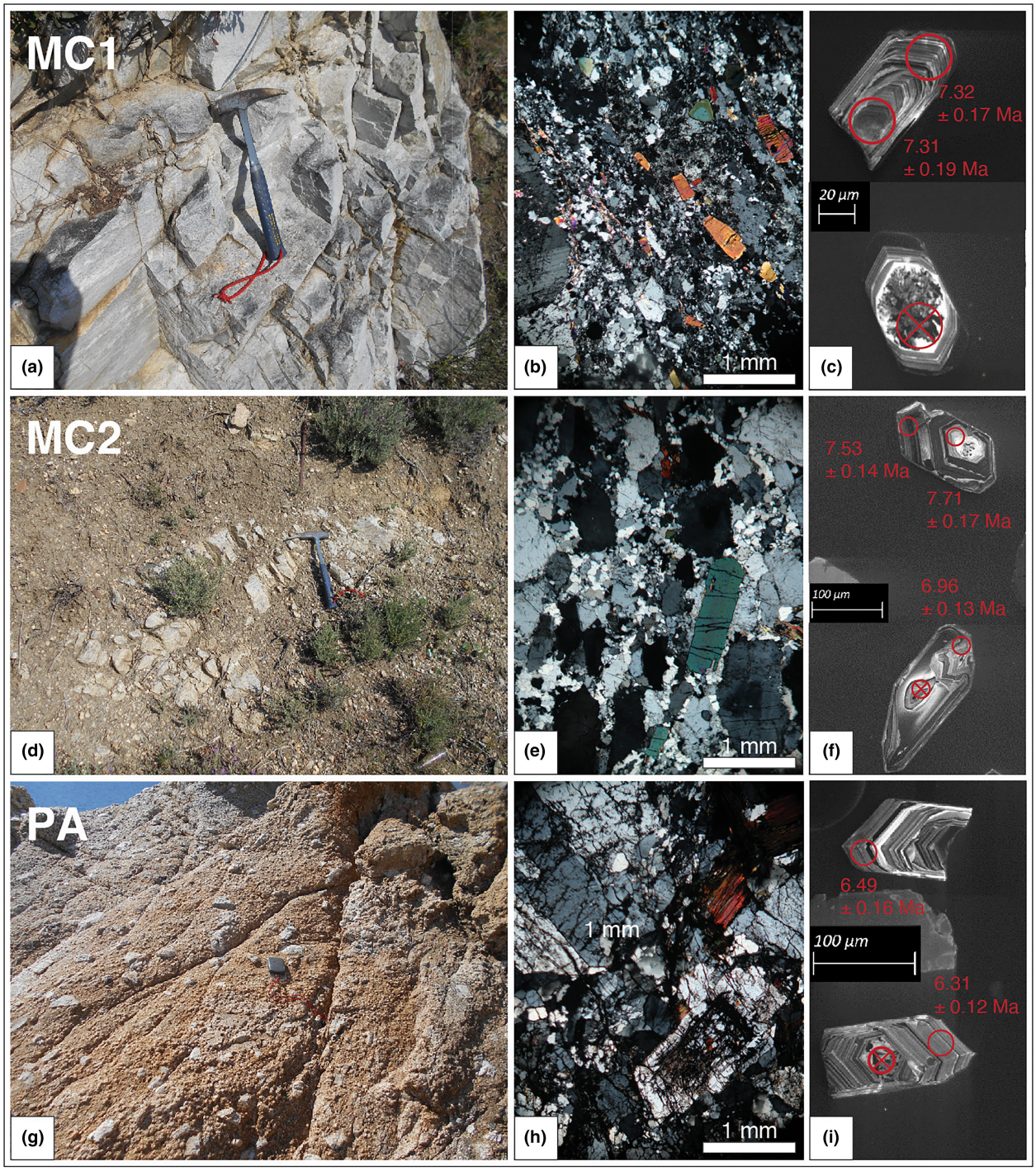


FIGURE 2 Photographs of outcrops, microphotographs of thin sections (X polars) and representative SEM CL-images of zircons for samples MC1 (a–c), MC2 (d–f) and PA1 (g–i). Red circles on CL-images: location of LA spots (diameter: 25 µm); crossed circles: failed analyses (see text for details); >90% concordant $^{206}Pb/^{238}U$ dates ±2s are indicated.

the scatter in the data to represent true geological variability (Figure 3; Figure S4).

Remarkably, the spread of zircon dates of our late-magmatic samples largely overlaps with the age spread in the main granite (SIMS data from Gagnevin et al., 2011 also represented), indicating that the late-stage dykes carry a record of zircon in a supersolidus melt continuing until ~7 Ma (our youngest MC rim being 6.96 ± 0.13 Ma, Figure 3). Similarly, the range of U–Pb zircon dates of PA1 overlaps with the spread of zircon dates determined on the PA monzogranite (Figure 3) by Spiess et al. (2021) and Gagnevin et al. (2011). Importantly, our zircon U–Pb data suggest that the two systems were active at the same time for at least 220 ka; that is the MC reservoir was still supersolidus during crystallization of the PA reservoir (Figure 4), the latter crystallizing zircon until ~6 Ma

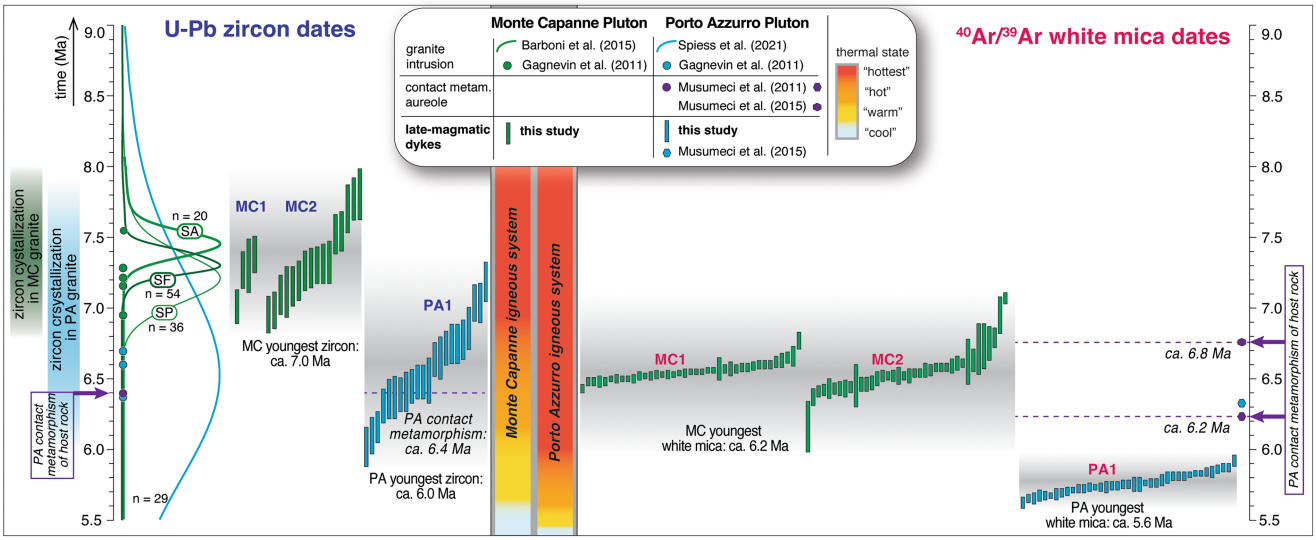


**FIGURE 3** Summary of U–Pb zircon ($^{206}Pb/^{238}U$ dates) and $^{40}Ar/^{39}Ar$ white mica data of the MC and PA igneous systems and host rock. Published U–Pb zircon data are plotted as normalized (adaptive) KDE diagrams (Vermeesch, 2018) Literature data from Spiess et al., 2021, LA ICP-MS concordant data; Barboni et al., 2015, ID-TIMS data; SA, Sant'Andrea; SF, San Francesco; SP, San Piero facies; Table S6. SIMS U–Pb individual zircon dates: Gagnevin et al., 2011; Musumeci et al., 2011; uncertainties not represented. $^{40}Ar/^{39}Ar$ w.m. weighted plateau ages: Musumeci et al., 2011, 2015. LA ICP-MS single zircon ablations and $^{40}Ar/^{39}Ar$ single fusion dates are plotted as ranked distributions (vertical bars: ±2s). Thermal state is qualitatively defined as: (i) 'hottest', allowing crystallization of new zircon in a supersolidus melt (with zircon saturation for the MC melts at $T \sim 800°C$, Barboni et al., 2015; in the absence of data, a similar $T$ is assumed for the PA melts) or overgrowth of metamorphic zircon in the aureole (Musumeci et al., 2011); (ii) 'hot', allowing limited mobility of the igneous body, emplacement of late-stage apophyses and dikes and rapid cooling as recorded by the $^{40}Ar/^{39}Ar$ isotopic system in w.m. ($\sim 800°C > T > \sim 400°C$); (iii) 'warm', representing cooling from hot conditions to the brittle–ductile transition (BTD, $T \sim 350°C$; Papeschi et al., 2017); (iv) 'cool' Ts below the BTD. See text for discussion and cf. Figure 4.

(youngest rim in PA1: 6.02 ± 0.14 Ma). This youngest PA crystallization recorded by the late-stage magmatism post-dates the thermal peak recorded in the PA contact aureole as indicated by a metamorphic zircon overgrowth in the Calamita Schist at 6.4 ± 0.2 Ma and by the thermal peak in the host rocks documented by $^{40}Ar/^{39}Ar$ white mica at 6.8 and 6.2 Ma (Musumeci et al., 2011, 2015). Altogether these data indicate that, after the main pluton had emplaced and metamorphosed the host rock, a melt reservoir remained available to allow continuous crystallization of zircon, as recorded by our late-stage PA1 sample (Figures 3 and 4).

Our single-grain $^{40}Ar/^{39}Ar$ age white mica distributions plot as simple Gaussian curves (peaking at 6.54 ± 0.01, 6.53 ± 0.01 and 5.78 ± 0.01 Ma, respectively MC1, MC2 and PA1) indicating fast cooling below the closure temperature shortly after emplacement (Figure S5).

Remarkably, for each of the three samples, the $^{40}Ar/^{39}Ar$ age distribution spreads across a range whose oldest end overlaps with (or closely follows) the youngest zircon dates in the same sample (Figure 3) as observed in long-living silicic reservoirs (e.g. Castellanos Melendez et al., 2023). The $^{40}Ar/^{39}Ar$ age distribution of sample MC2 includes a minor component at ~7.0 Ma, possibly pointing to incomplete isotopic resetting of very large white mica crystals during the fast cooling of the dyke, being the rate of chemical diffusion orders of magnitude lower than the rate of the thermal diffusion (e.g. Rout et al., 2021). A single fusion experiment at 8.4 Ma with a low radiogenic $^{40}Ar$ yields (~17%) could have derived from resorbed older wall rock, but is not considered as reliably dating the dyke emplacement.

Finally, we have modelled the post-emplacement cooling of a non-convecting intrusive sheet as a function of the intrusion thickness, host rock thermal diffusivity, latent heat during crystallization and the temperature difference between magma and host rock (e.g. Annen, 2011). The model results (Text S5) indicate that the 20 m thick PA1 apophysis cooled in <5 years to 30 years (respectively using a cold vs. hot host rock model, i.e. 300 vs. 600°C), while the 1 m thick MC dykes must have cooled in a few days to 4 weeks. The results of our modelling indicate that the youngest $^{40}Ar/^{39}Ar$ white mica dates in both the MC and PA samples constrain the timing of emplacement of the late-stage intrusions.

## 7 | LONG-LIVED MAGMA RESERVOIRS IN THE LATE MIOCENE THYRRENIAN CRUST

Our new U–Pb data testify to a zircon crystallization history recorded in the late magmatic products of both the Monte Capanne and Porto Azzurro igneous systems which overlaps with the ~1 Ma zircon crystallization record observed in the respective main granite bodies (Figure 3). This supports the protracted (although possibly not continuous, e.g. Barboni et al., 2015) occurrence at depth of sizeable long-lived reservoirs, feeding the main pluton body as well as the late-stage pulses.

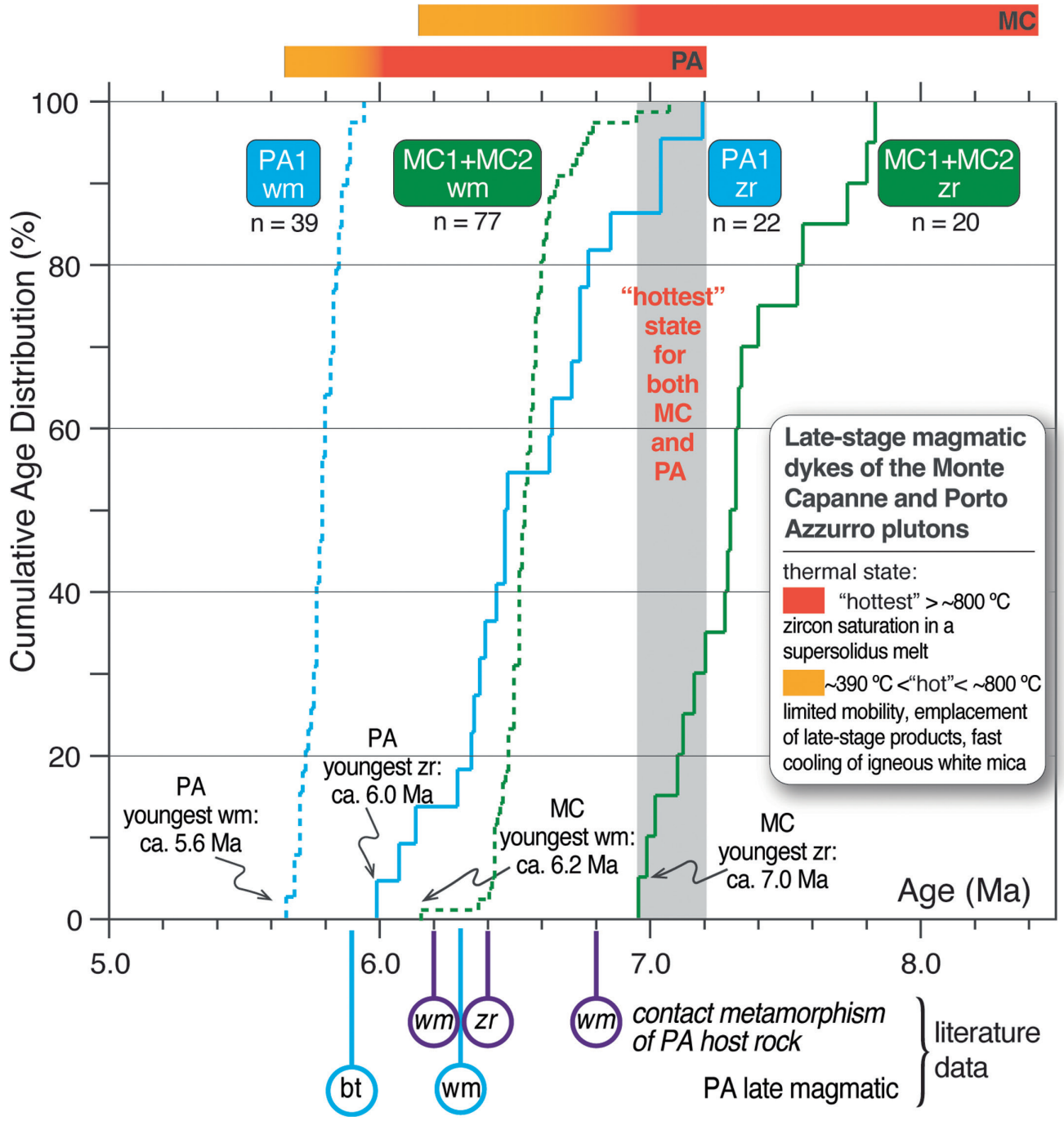


FIGURE 4 Cumulative age distributions (CAD) plots of U–Pb zircon ($^{206}Pb/^{238}U$ dates) and $^{40}Ar/^{39}Ar$ white mica age data. CAD diagrams do not consider the individual data uncertainties. The 'hottest' and 'hot' thermal states for PA and MC are qualitatively defined based on age data from this study (same as in Figure 3). Additional data from the literature (Table S6) are plotted for comparison. The grey band shows the ca 220 ka time interval when both MC and PA melts (feeding our late-stage magmatic samples) crystallized zircons.

Cooling through ~400°C by ~6.2 Ma (MC) and 5.6 Ma (PA), respectively, is constrained for the first time by our $^{40}Ar/^{39}Ar$ white mica data. Such cooling overlapped or closely followed youngest zircon crystallization in each pulse feeding our late-stage products, pointing to a supersolidus melt capable of crystallizing zircon until very shortly before emplacement and ruling out an antecrystic nature for at least the youngest zircon growth in all samples.

Remarkably, our U–Pb zircon data testify to coeval crystallization of new zircon for about 220 ka (~7.2 to 7.0 Ma) in both the MC and PA igneous systems (Figure 4). This is in contrast to the generally accepted view of a substantial temporal gap (~1 Ma) between the two upper crustal magmatic systems (e.g. Serri et al., 1993).

Further evidence for a long-lived PA reservoir is given by metamorphic white mica in the PA contact aureole at ~6.8 and ~6.2 Ma

and a zircon metamorphic overgrowth (~6.4 Ma) being post-dated by continuous igneous zircon crystallization in the reservoir until ~6.0 Ma (Figures 3 and 4).

The final post-emplacement cooling must have occurred very rapidly for the MC and PA dykes at the scale of years to days, as modelled by Papeschi et al. (2022) and this study (Text S5).

We conclude that the presence of two long-lived, sizeable magma reservoirs in both western and eastern Elba at supersolidus conditions at the same time (for ~200 ka around ~7.0 Ma) may indicate a relationship between the two systems in the late Miocene.

## ACKNOWLEDGEMENTS

The research was funded by FISR2016 INGV (PI: F. Galadini).

## DATA AVAILABILITY STATEMENT

Data are available on demand to the authors. The data used in this work are in the supplementary material.

## REFERENCES

Annen, C. (2011). Implications of incremental emplacement of magma bodies for magma differentiation, thermal aureole dimensions and plutonism–volcanism relationships. *Tectonophysics*, *500*(1–4), 3–10.

Annen, C., Blundy, J. D., Leuthold, J., & Sparks, R. S. J. (2015). Construction and evolution of igneous bodies: Towards an integrated perspective of crustal magmatism. *Lithos*, *230*, 206–221.

Bachmann, O., Miller, C. F., & de Silva, S. L. (2007). The volcanic–plutonic connection as a stage for understanding crustal magmatism. *Journal of Volcanology and Geothermal Research*, *167*, 1–23.

Barboni, M., Annen, C., & Schoene, B. (2015). Evaluating the construction and evolution of upper crustal magma reservoirs with coupled U/Pb zircon geochronology and thermal modeling: A case study from the Mt. Capanne pluton (Elba, Italy). *Earth and Planetary Science Letters*, *432*, 436–448.

Barboni, M., & Schoene, B. (2014). Short eruption window revealed by absolute crystal growth rates in a granitic magma. *Nature Geoscience*, *7*, 524–528.

Boccaletti, M., Elter, P., & Guazzone, G. (1971). Plate tectonics model for the development of the Western Alps and Northern Apennines. *Nature*, *234*, 108–111.

Bracciali, L. (2019). Coupled zircon–rutile U–Pb chronology: LA ICP-MS dating, geological significance and applications to sediment provenance in the Eastern Himalayan-Indo-Burman region. *Geosciences*, *9*(11), 467. https://doi.org/10.3390/geosciences9110467

Castellanos Melendez, M. P., Di Muro, A., Laurent, O., Kuiper, K., Wijbrans, J. R., & Bachmann, O. (2023). Explosive volcanism of Piton des Neiges (Reunion Island) and excess age dispersion in sanidine: Insights into magma chamber processes in a hotspot setting. *Chemical Geology*, *632*(121), 539. https://doi.org/10.1016/j.chemgeo.2023.121539

Cherniak, D. J., & Watson, E. B. (2000). Pb diffusion in zircon. *Chemical Geology*, *172*, 5–24.

Conti, P., Cornamusini, G., & Carmignani, L. (2020). An outline of the geology of the Northern Apennines (Italy), with geological map at 1:250,000 scale: Italian. *Journal of Geosciences*, *139*, 149–194.

Dini, A., Innocenti, F., Rocchi, S., Tonarini, S., & Westerman, D. S. (2002). The magmatic evolution of the late Miocene laccolith–pluton–dyke granitic complex of Elba Island, Italy. *Geological Magazine*, *139*, 257–279.

Dodson, M. H. (1973). Closure temperature in cooling geochronological and petrological systems. *Contributions to Mineralogy and Petrology*, *40*, 259–274.

Farina, F., Dini, A., Davies, J. H. F. L., Ovtcharova, M., Greber, N. D., Bouvier, A.-S., Baumgartner, L., Ulianov, A., & Schaltegger, U. (2018). Zircon petrochronology reveals the timescale and mechanism of anatectic magma formation. *Earth and Planetary Science Letters*, *495*, 213–223.

Farina, F., Dini, A., Innocenti, F., Rocchi, S., & Westerman, D. S. (2010). Rapid incremental assembly of the Monte Capanne pluton (Elba Island, Tuscany) by downward stacking of magma sheets. *Geological Society of America Bulletin*, *122*, 1463–1479.

Gagnevin, D., Daly, J. S., Horstwood, M. S. A., & Whitehouse, M. J. (2011). In-situ zircon U–Pb, oxygen and hafnium isotopic evidence for magma mixing and mantle metasomatism in the Tuscan Magmatic Province, Italy. *Earth and Planetary Science Letters*, *305*, 45–56.

Harrison, T. M., Celerier, J., Aikman, A. B., Hermann, J., & Heizler, M. T. (2009). Diffusion of $^{40}$Ar in muscovite. *Geochimica et Cosmochimica Acta*, *73*, 1039–1051.

Jackson, M. D., Blundy, J., & Sparks, R. S. J. (2018). Chemical differentiation, cold storage and remobilization of magma in the Earth's crust. *Nature*, *564*, 405–409. https://doi.org/10.1038/s41586-018-0746-2

Kaiser, J. F., de Silva, S., Schmitt, A. K., Economos, R., & Sunagua, M. (2017). Million-year melt–presence in monotonous intermediate magma for a volcanic–plutonic assemblage in the Central Andes: Contrasting histories of crystal-rich and crystal-poor super-sized silicic magmas. *Earth and Planetary Science Letters*, *457*, 73–86.

Lee, J., Williams, I., & Ellis, D. (1997). Pb, U and Th diffusion in natural zircon. *Nature*, *390*, 159–162. https://doi.org/10.1038/36554

Maineri, C., Benvenuti, M., Costagliola, P., Dini, A., Lattanzi, P., Ruggieri, C., & Villa, I. M. (2003). Sericitic alteration at the La Crocetta mine (Elba Island, Italy): Interplay between magmatism, tectonics, and hydrothermal activity. *Mineralium Deposita*, *38*, 67–86.

Miller, R. B., & Paterson, S. R. (2001). Construction of mid-crustal sheeted plutons: Examples from the North Cascades, Washington. *Geological Society of America Bulletin*, *113*, 1423–1442.

Musumeci, G., Mazzarini, F., & Cruden, A. R. (2015). The Zuccale fault, Elba Island, Italy: A new perspective from fault architecture. *Tectonics*, *34*, 1195–1218.

Musumeci, G., Mazzarini, F., Tiepolo, M., & Di Vincenzo, G. (2011). U–Pb and $^{40}$Ar–$^{39}$Ar geochronology of Palaeozoic units in the northern Apennines: Determining protolith age and alpine evolution using the Calamita Schist and Ortano Porphyroid. *Geological Journal*, *46*, 288–310.

Papeschi, S., Mazzarini, F., Musumeci, G., & Cruden, A. R. (2022). Emplacement of a felsic dyke swarm during progressive heterogeneous deformation, Eastern Elba Dyke Complex (Island of Elba, Italy). *Journal of Structural Geology*, *159*, 104600. https://doi.org/10.1016/j.jsg.2022.104600

Papeschi, S., Musumeci, G., Massonne, H. J., Bartoli, O., & Cesare, B. (2019). Partial melting and strain localization in metapelites at very low-pressure conditions: The northern Apennines magmatic arc on the Island of Elba, Italy. *Lithos*, *350*, 105230. https://doi.org/10.1016/j.lithos.2019.105230

Papeschi, S., Musumeci, G., & Mazzarini, F. (2017). Heterogeneous brittle–ductile deformation at shallow crustal levels under high thermal conditions: The case of a synkinematic contact aureole in the inner northern Apennines, southeastern Elba Island, Italy. *Tectonophysics*, *717*, 547–564.

Rocchi, S., Westerman, D. S., Dini, A., & Farina, F. (2010). Intrusive sheets and sheeted intrusions at Elba Island, Italy. *Geosphere*, *6*, 225–236.

Rosenbaum, G., & Lister, G. S. (2004). Neogene and quaternary rollback evolution of the Tyrrhenian Sea, the Apennines and the Sicilian Maghrebides. *Tectonics*, *23*, TC1013. https://doi.org/10.1029/2003TC001518

Rout, S. S., Blum-Oeste, M., & Wörner, G. (2021). Long-term temperature cycling in a shallow magma reservoir: Insights from sanidine

megacrysts at Taápaca volcano, Central Andes. *Journal of Petrology*, *62*(9), 1–32. https://doi.org/10.1093/petrology/egab010

Schaen, A. J., Jicha, B. R., Hodges, K. V., Vermeesch, P., Stelten, M. E., Mercer, C. M., Phillips, D., Rivera, T. A., Jourdan, F., Matchan, E. L., Hemming, S. R., Morgan, L. E., Kelley, S. P., Cassata, W. S., Heizler, M. T., Vasconcelos, P. M., Benowitz, J. A., Koppers, A. A. P., Mark, D. F., … Singer, B. S. (2020). Interpreting and reporting $^{40}Ar/^{39}Ar$ geochronologic data. *Geological Society of America Bulletin*, *133*, 461–487.

Serri, G., Innocenti, F., & Manetti, P. (1993). Geochemical and petrological evidence of the subduction of delaminated Adriatic continental lithosphere in the genesis of the Neogene–Quaternary magmatism of central Italy. *Tectonophysics*, *223*, 117–147.

Spiess, R., Langone, A., Caggianelli, A., Stuart, F. M., Zucchi, M., Bianco, C., Brogi, A., & Liotta, A. (2021). Unveiling ductile deformation during fast exhumation of a granitic pluton in a transfer zone. *Journal of Structural Geology*, *147*, 104326. https://doi.org/10.1016/j.jsg.2021.104326

Vermeesch, P. (2018). IsoplotR: A free and open toolbox for geochronology. *Geoscience Frontiers*, *9*, 1479–1493. https://doi.org/10.1016/j.gsf.2018.04.001

Villa, I. M. (2010). Disequilibrium textures vs equilibrium modelling: Geochronology at the crossroads. In M. I. Spalla, A. M. Marotta, & G. Gosso (Eds.), *Advances in interpretation of geological processes* (Vol. *332*, pp. 1–15). Geological Society, London, Special Publications.

Wotzlaw, J.-F., Schaltegger, U., Frick, D. A., Dungan, M. A., Gerdes, A., & Günther, D. (2013). Tracking the evolution of large-volume silicic magma reservoirs from assembly to supereruption. *Geology*, *41*, 867–870.

## SUPPORTING INFORMATION

Additional supporting information can be found online in the Supporting Information section at the end of this article.

**Data S1.**

**How to cite this article:** Mazzarini, F., Bracciali, L., Musumeci, G., Wijbrans, J. R., Kuiper, K., & Horstwood, M. S. A. (2024). Coupled U–Pb and $^{40}Ar/^{39}Ar$ chronology of late-stage intrusions at Elba Island (Italy) supports late Miocene long-lived magma reservoirs in the Tyrrhenian upper crust. *Terra Nova*, *00*, 1–8. https://doi.org/10.1111/ter.12706